



HAL
open science

Magnetic Tunnel Junction Applications

Nilson Maciel, Elaine Marques, Lirida Naviner, Yongliang Zhou, Hao Cai

► **To cite this version:**

Nilson Maciel, Elaine Marques, Lirida Naviner, Yongliang Zhou, Hao Cai. Magnetic Tunnel Junction Applications. Sensors, 2020, 20 (1), pp.121. 10.3390/s20010121 . hal-02941339

HAL Id: hal-02941339

<https://hal.science/hal-02941339>

Submitted on 26 Jan 2024

HAL is a multi-disciplinary open access archive for the deposit and dissemination of scientific research documents, whether they are published or not. The documents may come from teaching and research institutions in France or abroad, or from public or private research centers.

L'archive ouverte pluridisciplinaire **HAL**, est destinée au dépôt et à la diffusion de documents scientifiques de niveau recherche, publiés ou non, émanant des établissements d'enseignement et de recherche français ou étrangers, des laboratoires publics ou privés.

Review

Magnetic Tunnel Junction Applications

Nilson Maciel ^{1,*}, Elaine Marques ¹, Lírída Naviner ¹, Yongliang Zhou ²  and Hao Cai ²

¹ LTCI, Télécom Paris, Institut Polytechnique de Paris, 91128 Palaiseau, France; ecrespo@telecom-paris.fr (E.M.); lirida.naviner@telecom-paris.fr (L.N.)

² National ASIC System Engineering Center, Southeast University, Nanjing 210096, China; zhouyongliang@seu.edu.cn (Y.Z.); hao.cai@seu.edu.cn (H.C.)

* Correspondence: nmaciel@telecom-paris.fr

Received: 15 November 2019; Accepted: 20 December 2019; Published: 24 December 2019



Abstract: Spin-based devices can reduce energy leakage and thus increase energy efficiency. They have been seen as an approach to overcoming the constraints of CMOS downscaling, specifically, the Magnetic Tunnel Junction (MTJ) which has been the focus of much research in recent years. Its nonvolatility, scalability and low power consumption are highly attractive when applied in several components. This paper aims at providing a survey of a selection of MTJ applications such as memory and analog to digital converter, among others.

Keywords: magnetic tunnel junction; spin transfer torque; spin-orbit torque; voltage-controlled magnetic anisotropy; magnetic random access memory

1. Introduction

The discovery of Giant Magnetoresistance (GMR) [1,2] led to the development of spintronics [3]. Studies in this area have resulted in several important advances. With CMOS downscaling, the need of viable alternatives for reducing the leakage of power increases and spin-based devices appear as one of the most promising approaches to deal with this issue.

Magnetic Tunnel Junction (MTJ) has a significant role in the spintronics development [4]. Its structure has ferromagnetic layers connected with a insulator layer between them. MTJ has excellent scalability, low power consumption and potentially infinite endurance. In addition, unused MTJs can be completely powered off without the loss of data resulting in saving energy which render the MTJ suitable for several applications [4] such as memory devices and analog to digital converter. MTJ-based non-volatile memories (NVMs) have shown superior performance with respect to many relevant figure of merits such as energy efficiency and endurance [5]. MTJ-based memories allow for a ten year retention time operating at extremely low energy levels making them appropriate for batteries or low powered applications as internet of things (IoT) applications, specifically for sensor nodes located in difficult environmental conditions [6].

MTJ applications can also be found in several domains where data require processing and storage [7–10]. In radio frequency, spectrum-optimizing applications based on compressive sensing [11] desire to reduce the area of their circuits and decrease power consumption. In order to do this, MTJs can be used in mixed signal applications, such as comparators and analog to digital converters [9,10].

Recently, relevant progress has been done in MTJ research and it is expected to develop even further into commercial products in the near future. In order to help engineers and researchers who are just starting to work with MTJs or who are interested in learning about its wide and diverse application fields, this paper reviews important MTJ works reported in the literature over the last years.

The rest of the paper is organized as follows. Section 2 briefly explains the MTJ while also presenting STT, VCMA and SOT. The MTJ's properties allows it be applied in several structures.

Some of the most important digital applications are discussed in Section 3. On the other hand, Section 4 addresses some mixed and analog applications where MTJs can be found. Finally, Section 5 concludes the work.

2. Magnetic Tunnel Junction (MTJ)

Figure 1 illustrates the basic MTJ structure. It consists of two ferromagnetic layers separated by the insulator layer MgO. The reference layer has unchangeable magnetization direction, while the magnetization direction can be changed in the free layer. Therefore, the magnetic field determines electrical properties of the MTJ. For applications, the difference of the conductance, resulted from the variations of the magnetic field in the ferromagnetic layers, is employed. The magnetization orientations (m_z) of the two ferromagnetic layers are related to a level of the MTJ resistance: low-resistance R_P at a parallel state and high-resistance R_{AP} at an anti-parallel state. With these two stable states of the MTJ, it can be easily used to represent logic 0 or logic 1 [12–15].

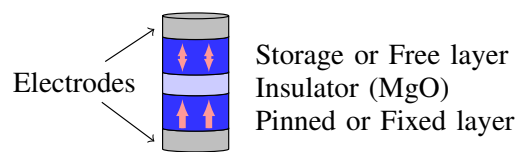


Figure 1. Magnetic tunnel junction (MTJ).

In order to control the electrical characteristics of MTJs, some methods have been developed for switching their stable states. The three main MTJ magnetization switching mechanisms are discussed below.

2.1. Spin Transfer Torque (STT)

Spin transfer torque was presented in Reference [16] as an alternative to improve the density of the first proposed MTJ circuits. The STT effect allows switch the MTJ state by a bidirectional current I when the current is bigger than a critical current I_{c0} . It improves the scalability of the circuit with MTJs allowing a denser layout and a simpler design due the use of the same line to write and read the MTJ state. However, using the same path can lead to unexpected writing when reading is in progress. Another disadvantage of the STT is that the current required to switch the states of the MTJ is not symmetrical (going from P to AP requires a bigger current than going from AP to P). Moreover, when using STT, a larger access transistor size is required, thus limiting the application density. Yet another challenge with scaling down using STT is that the thermal stability factor scales down linearly with the area and the increase in retention failures due to thermal instability results in unreliable operations [17]. STT-based applications also face problems when high write speed is required because the switching current of STT is inversely proportional to the write pulse width [17].

The MTJ behavior model is given by [18,19]:

$$I_{c0} = \alpha \frac{\gamma e}{\mu_B g} (\mu_0 M_s) H_k V \quad (1)$$

$$E = \frac{\mu_0 M_s H_k V}{2}, \quad (2)$$

where α is the magnetic damping constant, γ is the gyromagnetic ratio, e is the elementary charge, μ_B is the Bohr magneton, g is the spin polarization efficiency factor, μ_0 is the permeability of free space,

M_s is the saturation magnetization, H_k is the effective anisotropy field and V is the volume of the free layer. Equation (3) gives the average MTJ state switching delay time (τ) [18,19].

$$\tau = \tau_0 \exp\left(\frac{E}{k_B T} \left(1 - \frac{I}{I_{c0}}\right)\right), \text{ when } I < I_{c0} \quad (3)$$

$$\frac{1}{\tau} = \left[\frac{2}{C + \ln\left(\frac{\pi^2 \epsilon}{4}\right)} \right] \frac{\mu_B P_{ref}}{em_m (1 + P_{ref} P_{free})} (I - I_{c0}), \text{ when } I > I_{c0}, \quad (4)$$

where τ_0 is the attempt period, k_B is the Boltzmann constant, T is the temperature, C is Euler's constant, ϵ is the thermal stability factor, m_m is the magnetization moment, P_{ref} and P_{free} are the tunneling spin polarizations.

2.2. Voltage-Controlled Magnetic Anisotropy (VCMA)

Magnetoelectric effects have been studied with the aim at efficiently switching the MTJ state consuming less energy [20]. Efficient energy consumption and reduced area can be achieved if a voltage-controlled MTJ with an electric field (or a voltage) is used [21,22]. With the VCMA effect, an electric field is used in order to switch the MTJ state. It occurs by an accumulation of electron charges induced by the electric field changing the occupation of atomic orbitals at the interface. This and the spin-orbit interaction lead to a change of magnetic anisotropy [20,23,24].

Figure 2 outlines the VCMA-MTJ operational characterization. As the switching is performed through voltage, the increasing of the barrier thickness can decrease the parasitic conductance and so the effect of current-induced torques [17]. The energy barrier between the P and AP states can be reduced with the use of VCMA. Therefore, a voltage applied across the MTJ terminals facilitates the switch of its states. When the MTJ critical voltage V_c is smaller than the switching voltage V_b , the energy barrier E_b between two stable magnetization states can be eliminated. Equation (5) gives the minimum V_c for successful VCMA-MTJ switching [25]:

$$V_c = \Delta(0) k_B T t_{ox} / \xi A, \quad (5)$$

where ξ is the VCMA coefficient to weigh the perpendicular magnetic anisotropy (PMA) change under V_b , $\Delta(0)$ is the thermal stability under zero voltage, A is the sectional area of the MTJ, T is the temperature, t_{ox} is the MTJ oxide layer thickness and k_B is the Boltzmann constant.

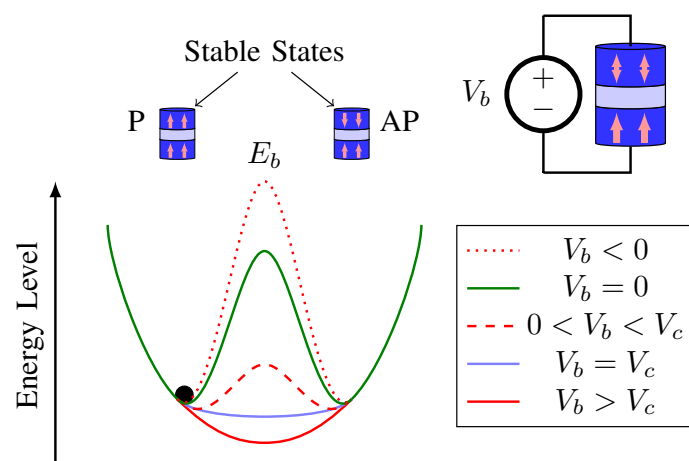


Figure 2. Structure and stable states of the voltage-controlled magnetic anisotropy (VCMA)-MTJ device.

The VCMA-MTJ dynamics changes continuously through its unstable states, once V_c is achieved [26]. The E_b of the intermediate states comes back to a greater value than the stable states leading to stabilize the MTJ in its P or AP state when the excitation of its terminals has finished.

Compared to STT, VCMA does not require large currents facilitating the scalability of its applications and resulting in a lower power consumption. However, practical VCMA devices face reliability issues which have to be better understood [27].

2.3. Spin-Orbit Torque (SOT)

With the SOT technique, three terminals are used to separate the write and read paths allowing for a symmetrical switching current between the MTJ states. With that, the possibility of a bit flip during the read operation is reduced, therefore increasing the read stability [17]. When a current crosses the non-magnetic layer, spins are accumulated and a torque switching is generated over the magnetization of the ferromagnetic layer. A faster switching can occur using SOT with the elimination of the time-demanding precessional motion [28]. However, one disadvantage of SOT is that it requires bigger cell size than STT-based applications due to its three terminal structure, so it can be not compatible with high-density applications.

3. Digital Applications

This sections addresses some MTJ-based digital applications.

3.1. Memory

One of the most known MTJ applications is the MTJ-based memory. Magnetic Random-Access Memory (MRAM) aims at combining the best characteristics of dynamic random-access memory (DRAM), static random-access memory (SRAM) and flash memory in order to become the “universal memory” [29,30]. Using the intrinsic spin of electrons as a storage unit and the difference of the MTJ resistance in its parallel and antiparallel states to represent the “0” and “1” in the binary system, MTJs are applied as the basic elements in information storage.

The structures of MTJ-based MRAM differ in the write operation approach and the number of MOS transistors [31–34] used to build a unit cell of memory. Figure 3a illustrates the spin transfer torque MTJ-based MRAM (STT-MRAM) bit-cell structure. Each bit-cell has only one transistor with the STT-MTJ allowing higher density memories. As it is shown in Figure 3a, while the bi-directional current I_w is responsible for switching the MTJ state during the write operation, the MTJ state is defined comparing the read current I_r with a reference current [15]. It is worth mentioning that STT-MRAM is characterized by an asymmetric write operation. This occurs because the current required to switch from the AP to P state is smaller than that of switching from the P to AP state [33]. Therefore, in order to achieve the requirement of worse case of the write operations, the access transistor has to be large [32,33,35].

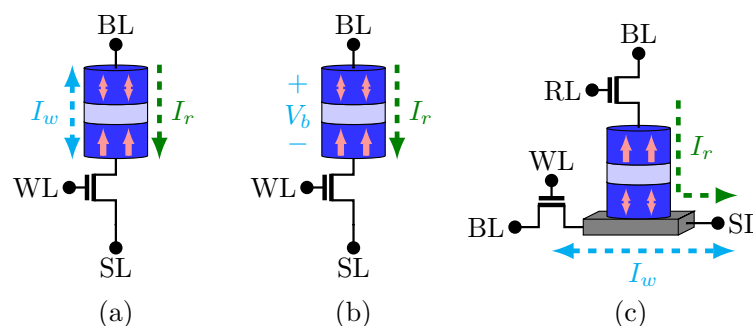


Figure 3. Memories devices: (a) STT-MRAM (b) VCMA-MeRAM (c) SOT-MRAM.

Furthermore, STT-MRAM has intrinsic problems in terms of long latency and high write power when compared with other mechanisms [26]. On the other hand, MTJ with VCMA provides magnetization flipping upon a voltage pulse [21,36]. Using voltage for writing data into an MTJ instead of a charge current can result in a lower energy dissipation [26]. Moreover, the required

driving current decreases for the write operation allowing a reduction of the access transistor size [26]. VCMA-MTJ-based memory performs better than STT-MRAM with respect to switching energy and density [20,26,37,38].

The VCMA-MeRAM structure is illustrated in Figure 3b. Just like STT-MRAM, it has 1 MTJ and 1 access transistor in series. Its write operation consists of either maintaining the MTJ state or switching it. An extra circuit is responsible for checking the MTJ state and deciding to switch or maintain the MTJ state.

Another structure is the SOT-MRAM. Its bit-cell design is represented in Figure 3c. As can be seen, its integration density capacity is reduced due to the two access transistors in each bit-cell [32,34]. In this MTJ-based MRAM, the write path and the read path are different. The write current I_w is generated by the voltage applied between the source line (SL) and the bit line (BL). It is polarized and it switches the magnetization direction of the MTJ free layer. On the other hand, during the read operation, the MTJ state is read according to the magnitude of I_r [39].

Some works suggest that SOT-MRAM requires a lower write time and a lower write energy than STT-MRAM [40–43]. On the other hand, the results presented in Reference [26] show that VCMA-MeRAMs outperform STT-MRAM in terms of area, speed and energy consumption. Table 1 reproduces some comparisons presented in Reference [44]. However, it should be highlighted that they are developing technologies. Even if products based in STT MTJ is already in commercialization, intensive research and development are being done in this field especially regarding VCMA and SOT.

Table 1. Comparison between some MTJ-based memories.

	STT-MRAM	SOT-MRAM	VCMA-MeRAM
Read Time (ns)	1–5	1–5	1–5
Write Time (ns)	5–10	<1	<1
Cell Size (area in F^2)	40–50	50–70	20–30
Bit Density (Gb/cm ²)	1	0.75	2
Read Energy/Bit (fJ)	10–20	10–20	1–5
Write Energy/Bit (fJ)	100–200	<10	<5

Some other memories using multiples mechanisms to write and read MTJ device have also been proposed. NAND-SPIN is an example of MTJ-based memory [32] which uses more than one of the cited switching mechanisms (see Figure 4). The idea is to take advantages of both STT and SOT mechanisms, while aiming at better performance. Compared to SOT-MRAM, NAND-SPIN memory has a better integration density. It occurs because the transistors are shared by several MTJs. On the other hand, compared to STT-MRAM, NAND-SPIN leads to better energy performance [32].

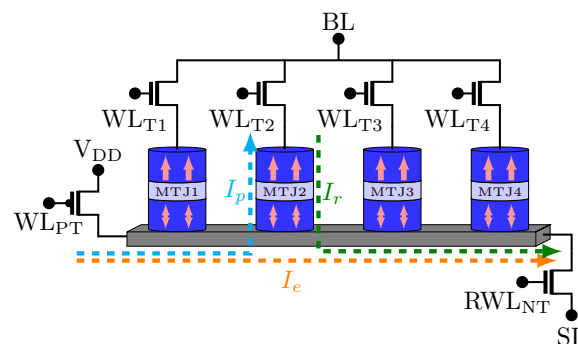


Figure 4. 4-bit NAND-SPIN structure.

Figure 5 illustrates the timing diagram for the write and read operations over MTJ2. As can be noticed, the write operation of the NAND-SPIN has two phases:

- Erase: this phase initializes the MTJs at their AP states. Moreover, the transistors NT and PT are on, while the access transistors are off. Then, a write current I_e goes through the shared metal strip.
- Program: in this phase, the transistor PT and the corresponding access transistor are on (for the case represented in Figure 5, the corresponding access transistor is T2). Therefore, a current I_p flows through the MTJ from the free layer to the pinned layer switching the MTJ state to P by the STT mechanism.

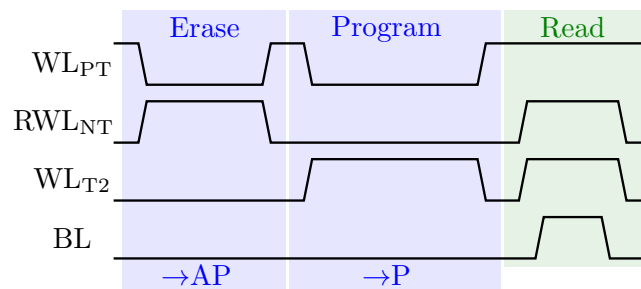


Figure 5. Timing diagram of write and read operations for the NAND-SPIN over MTJ2.

During the read operation, the access transistor corresponding to the MTJ which will be read and the transistor NT are on. The reading of the MTJ state is made by comparing a reference current with I_r .

Even if MTJ has high tolerance to radiation [45], the MOS access transistors in MTJ-based memory structures may be impacted by radiation. Among other factors, tolerance to radiation is one important and studied field [46–49] when it is necessary to take into account performance and risks of MRAM in the integration process of MOS technology.

3.2. Logic Gates

Non-volatile logic gates are other MTJ applications which allow for the reduction in area and power consumption.

Figure 6 illustrates the NV-AND / NV-NAND structure. Q and \bar{Q} represent AND and NAND operations, respectively. The truth table is given by Table 2 and the logic functions are illustrated by (6) and (7). This structure gives correct functions for any resistive level of MTJ.

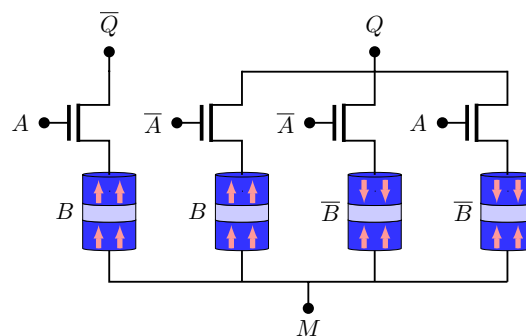


Figure 6. NV-AND / NV-NAND structure.

Table 2. Truth table of AND/NAND.

A	B	Q (AND)	\bar{Q} (NAND)
0	0	0	1
0	1	0	1
1	0	0	1
1	1	1	0

$$Q = AB \tag{6}$$

$$\bar{Q} = \bar{A}\bar{B} = \bar{A} + \bar{B} = \bar{A}B + A\bar{B} + \bar{A}\bar{B} \tag{7}$$

The NV-OR / NV-NOR structure is shown in Figure 7. Q and \bar{Q} represent OR and NOR operations, respectively. The truth table is given by Table 3 and the logic functions are illustrate by (8) and (9).

$$Q = \bar{A}B + A\bar{B} + AB \tag{8}$$

$$\bar{Q} = \bar{A}\bar{B}. \tag{9}$$

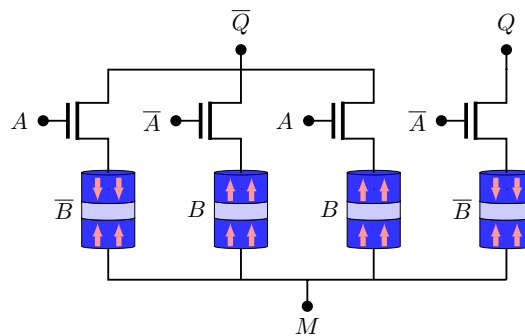


Figure 7. NV-OR / NV-NOR structure.

Table 3. Truth table of OR/NOR.

A	B	Q (OR)	Q̄ (NOR)
0	0	0	1
0	1	1	0
1	0	1	0
1	1	1	0

Figure 8 presents the NV-XOR / NV-NXOR structure. Q and \bar{Q} represent XOR and NXOR operations, respectively. The truth table is given by Table 4 and the logic functions are illustrate by (10) and (11).

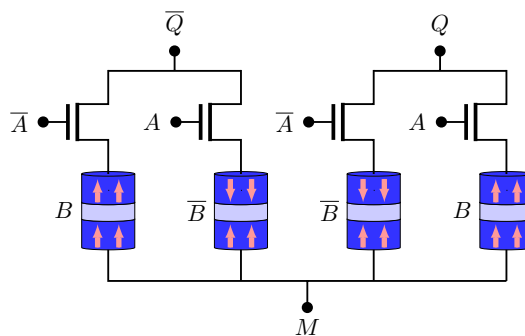


Figure 8. NV-XOR / NV-NXOR structure.

Table 4. Truth table of XOR/NXOR.

A	B	Q (XOR)	\bar{Q} (NXOR)
0	0	0	1
0	1	1	0
1	0	1	0
1	1	0	1

$$Q = \bar{A}B + A\bar{B} \quad (10)$$

$$\bar{Q} = \bar{A}\bar{B} + AB \quad (11)$$

In Reference [50], the author proposes some logic gate structures that reduce the number of NMOS transistors and the MTJ when compared with the logic gate structures presented. However, for their proper operation, some NMOS and MTJ settings must be followed such as their resistance configurations.

3.3. Look-up Table (LUT)

One of the main components of FPGAs are Look-Up Tables (LUTs) which are usually composed by SRAM cells [51]. Nevertheless, SRAM-based LUTs have limitations such as low logic density, volatility and high static power [52]. On the other hand, in MTJ-based LUT only the data processing portion is active, whereas other parts are powered off reducing the power consumption and mutual disturbance.

Table 5 reproduces the comparison of some MTJ-based LUTs presented in Reference [53]. While the spin-based LUTs presented in References [53–57] require a clock, in Reference [52], a 6-input fracturable non-volatile Clockless LUT (C-LUT) using a spin Hall effect (SHE)-based MTJ is proposed for combinational logic operations without needing a clock. This C-LUT eliminates the sense amplifier generally employed and decreases the area compared to the STT-MTJ-based C-LUT.

Table 5. Characteristics of LUT designs.

Design	Write/Read Operation	Features and Challenges
FIMS-LUT [58]	Magnetic Field/TMR	High Speed High Power Consumption High Area Overhead
TAS-LUT [54]	Magnetic Field/TMR	Relatively High Speed High Power Consumption Medium Area Overhead
STT-LUT [53]	STT/TMR	High Speed Low Power Consumption Low Area Overhead
A-LUT [53]	STT/TMR	High Speed Scalable Power Consumption Low Area Overhead

3.4. Flip-Flop (FF)

The loss of the data due to power failures and system crashes can be avoided using flip-flop based on non-volatile memory. In Reference [59], one of the first non-volatile flip-flop based on MTJ for FPGA and System On Chip (SoC) circuits is proposed. All the data processed is permanently stored in the Spin-MTJ memory cells making these circuits fully non-volatile. Figure 9 illustrates its full schematic, that is, the sense amplifier with the bidirectional current source.

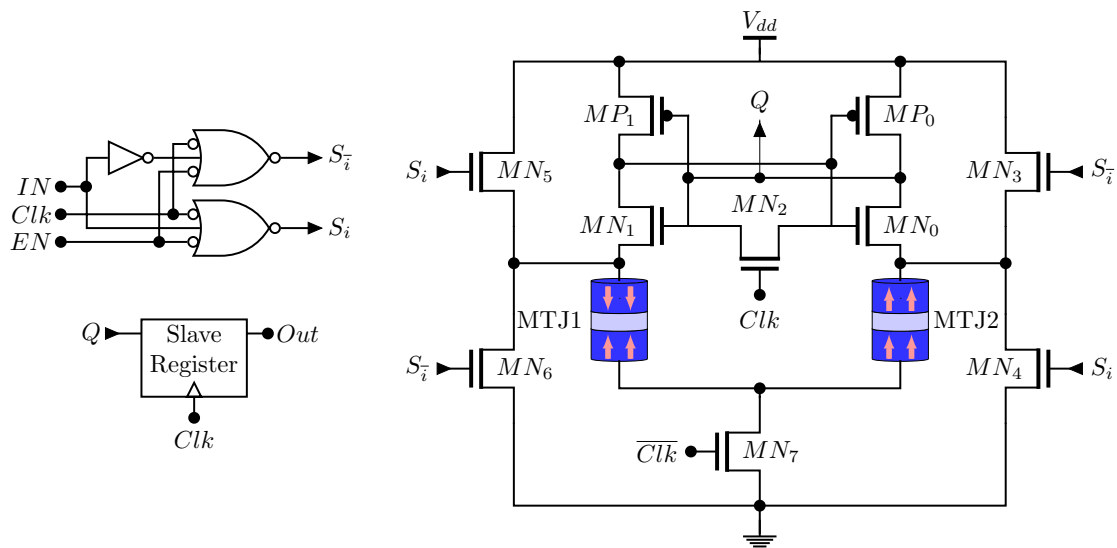


Figure 9. Spin-MTJ based Non-Volatile Flip-Flop proposed in Reference [59].

The NOR gates control the activation of the transistors MN3, MN4, MN5, MN6. Each time, two of them are active. The signal EN enables the current source thus reducing the power dissipation as the circuit is in static mode. The signal IN writes the pair of MTJs and gives the current direction. MN7 switches between the writing and reading mode. When $Clk = 1$, the slave register keeps the previous data and the input data is stored. On the other hand, when $Clk = 0$, the data stored is read by the sense amplifier and the slave register updates with Q. Other non-volatile flip-flop implementations can be found in References [19,60–62].

3.5. Full Adder (FA)

Figure 10 illustrates a single-bit full adder structure. It consists of three inputs (A , B and C_i) and two outputs (S and C_o) given by (12) and (13). FA is a basic unit to an arithmetic operation in a CPU. Low-power and high-density FA are desirable.

$$S = A \oplus B \oplus C_i = ABC_i + A\bar{B}\bar{C}_i + \bar{A}B\bar{C}_i + \bar{A}\bar{B}C_i \tag{12}$$

$$C_o = AB + AC_i + BC_i \tag{13}$$

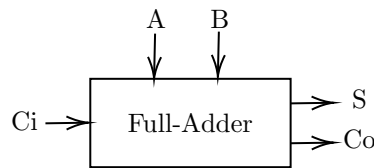


Figure 10. Single-bit full adder (FA) schematic.

Figure 11 presents the SUM and the CARRY sub-circuits proposed with MTJ elements [50]. Several other non-volatile full adders were proposed in References [8,63–65].

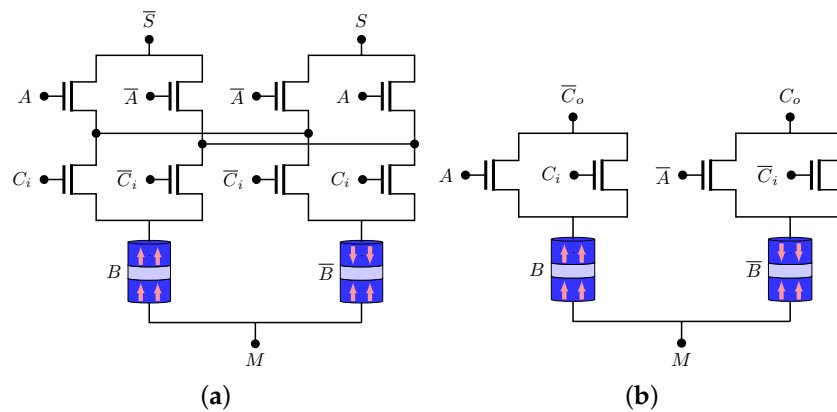


Figure 11. Full adder structure: (a) SUM sub-circuit (b) CARRY sub-circuit.

4. Mixed and Analog Applications

This sections addresses MTJ-based mixed and analog applications.

4.1. Comparator

One of most important components of an ADC is the comparator. A low-power and high-speed comparator is essential to build a high-speed ADC. Traditional comparators have several stages of latches and amplifiers [66].

In Reference [67], an MTJ comparator is proposed using one transistor and one spin Hall driven MTJ (see Figure 12). The spin Hall metal (SHM) is in contact with the free layer of the MTJ. Consequently, a spin current transversely can be produced by a charge current flowing in the SHM, hence applying spin-transfer torque on the free layer for switching.

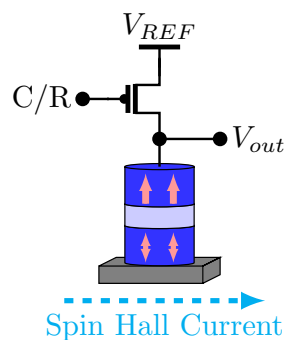


Figure 12. Comparator proposed in Reference [67].

4.2. Analog to Digital Converter (ADC)

The ADC poses many challenges depending on its application. For example, compact ADCs could be important in parallel data conversion for image processing [68]. Furthermore, with the downscaling of CMOS, the increased static energy consumption has to be avoided. The traditional architecture and operation mode of the ADCs are not suitable for improvement on resolution and power consumption [66,69]. New technologies and new device design are required to meet the demands of IoT devices, cognitive radios and other applications in terms of ADC constraints related to sampling rate, area, power consumption and bandwidth [67]. Even if a lot of data converters are based on CMOS [70], in recent years, spintronic devices have been explored in order to save area and reduce the power consumption of the ADCs [10,67,68].

In Reference [67], the comparator illustrated in Figure 12 is used to design a 3-bit spin-based ADC (see Figure 13). It can be noticed that 8 comparators are used to provide a 3-bit resolution.

The conversion is composed of three phases: reset, conversion and read. Figure 14 shows the timing diagram of ADC operations. During the reset phase, all MTJs go to their AP state. In the conversion phase, the transistors are on. The voltages on MTJs are different due to the resistors. The VCMA effect in MTJ results in the increase of switching currents from left to right on the comparator, leading to bit levels. A pulse on EN1 samples the input signal and transmits it through the SHM, thus switching some of the MTJs. Finally, in the read phase, the transistors are off and the results are read. This ADC presents improvements in terms of power consumption compared to Flash ADC presented in the literature [67].

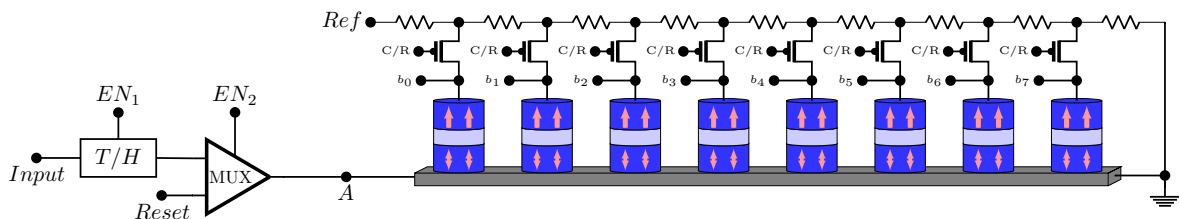


Figure 13. ADC proposed in Reference [67].

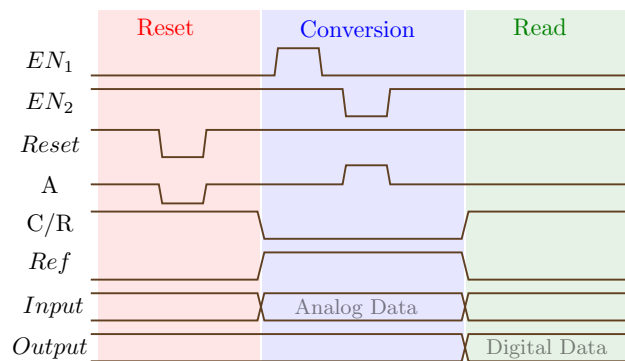


Figure 14. Timing diagram of the ADC operations [67].

In order to do approximate analog to digital conversion at low voltages, a voltage-controlled stochastic switching device based on a superparamagnetic nanomagnet is proposed in Reference [10]. Figure 15 illustrates the schematic of the ADC. It is composed by a counter, two MTJs and two back-to-back inverters. As shown, the analog input enters in the ME oxide terminal of the MTJ and the counter output gives the digital output. When the input voltage increases, the probability of the MTJ2 in the AP state increases too. When the MTJ2 is in its AP state $C_{in} = 1$, otherwise $C_{in} = 0$. At the positive edge of the clock, the counter counts up if $C_{in} = 1$. Finally, the digital count is translated to a binary code through look-up-tables. The results of Reference [10] show that the proposed ADC is suitable for sensors which require low-voltage conversions. Moreover, compact and lower power can be achieved using this proposition.

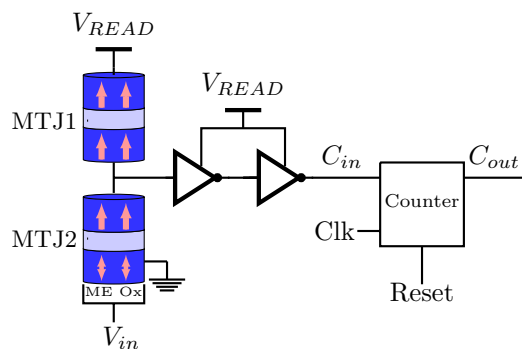


Figure 15. ADC proposed in Reference [10].

4.3. Non-Uniform Clock Generator

Non-uniform sampling (NUS) analog-to-information converters (AIC) generally have a non-uniform clock generator. Normally, a pseudo-random generator Linear Feedback Shift Register (LFSR) integrates an asynchronous clock generator used in non-uniform sampling techniques to randomly select a clock signal. However, this circuit can require a large number of CMOS transistors leading to significant power dissipation and area consumption.

In Reference [71], the authors propose a non-uniform clock using VCMA-MTJs which outperforms the CMOS-based ones in terms of area and power. Figure 16 illustrates the MTJ-based voltage-controlled stochastic oscillator (VCSO) proposed in Reference [71]. The voltage V_B is related to the maximum frequency of an analog input signal. M1, M2 and M3 are responsible for maintaining the voltage on the N1 node independent of the variations of the MTJ resistance. With that, V_B direct defines the voltage across the MTJ controlling its switching rate. In other words, V_B increases if the input signal frequency is high. This will reduce the MTJ energy barrier, resulting in a higher rate of state switching. On the other hand, when the input signal frequency is low, V_B is also low and the MTJ energy barrier continues to be high, reducing the state switching rate. The MTJ's resistance is sensed by the amplifier. After that, a voltage variation on the N3 node related to the MTJ's resistance fluctuation is amplified. Finally, the N4 node is sent to a buffer in which an asynchronous ADC is connected to.

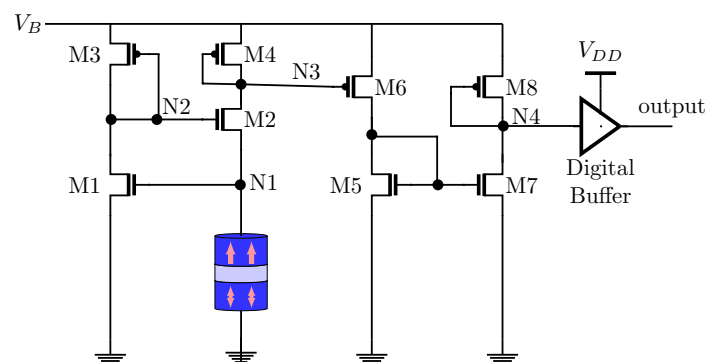


Figure 16. The MTJ-based voltage-controlled stochastic oscillator (VCSO) proposed in Reference [71].

It can be noticed that the amount of transistors is drastically reduced using the VCMA-MTJ instead of the traditional CMOS-based non-uniform clock generators. However, this generator considers the signal's frequency to generate the sampling clock. Therefore, it is not suitable for signals where their frequency is unknown or those with a large bandwidth.

On the other hand, the non-uniform clock generator using MRAM-based stochastic oscillator devices called Adaptive Quantization Rate (AQR) generator proposed in Reference [72] takes into account the signal's sparsity to generate the sampling clock. Thus, the number of samples is reduced leading to more energy savings.

Figure 17 illustrates the AQR. The stochastic behavior of the VCMA-MTJ provides the non-uniform clock generation capability. The voltage V_{SR} is related to the signal's sparsity that can be known or can be estimated before. Therefore, the V_{SR} applied to the NMOS of the AQR will generate a stochastic bit-stream by the MRAM-based stochastic oscillator device [72]. The Asynchronous Clock (A-Clk) is given by the result of the NAND gate between the actual clock and the output of the D-Flip-Flop (D-FF). It can be noticed that using AQR, large LFSR circuits which has many multiplexers, logic gates and D-FFs are avoided.

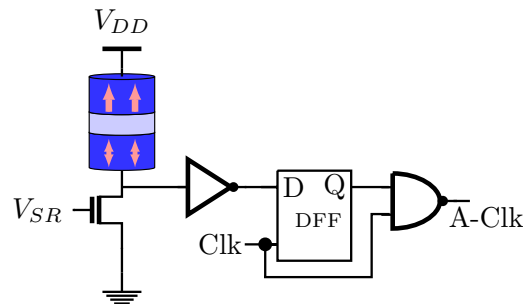


Figure 17. Adaptive Quantization Rate (AQR) generator proposed in Reference [72].

4.4. Adaptive Intermittent Quantizer (AIQ)

In Reference [9], the authors propose a Spin-based Adaptive Intermittent Quantizer (AIQ) in order to have an adaptive signal sample and quantization. Compressive sensing (CS) theory and spin-based devices are applied for energy-aware acquisition of spectrally sparse signals. Compared to conventional CMOS designs, the use of VCMA-MTJ allows reducing the energy consumption via an instant on/off operation. It does not require the use of a backing store and it leads to a fast sampling rate (SR), an adaptive quantization resolution (QR) and area reduction.

Figure 18 shows the Q-level AIQ architecture proposed in Reference [9], where Q is the number of QR levels. The quantization levels of the AIQ are given by changes in the energy barrier of the VCMA-MTJs.

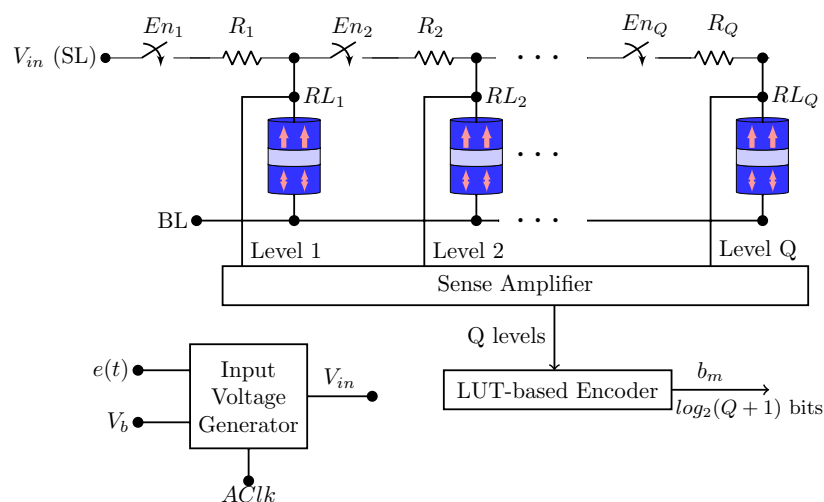


Figure 18. Q-level adaptive intermittent quantizer (AIQ) architecture proposed in Reference [9].

There are three main steps during the AIQ operation [9]:

- **Reset:** all active VCMA-MTJs go to their parallel state, that is, they are reset to zero. In order to do this, the source line (SL) is set to “0”, bit line (BL) is set to “1” and read lines (RLs) are in high impedance.
- **Sampling:** the active VCMA-MTJs are written. In other words, the energy barrier of the active VCMA-MTJs are modified and set by the bias voltage V_b applied across the active VCMA-MTJs followed by the analog input $e(t)$. The sampling rate of $e(t)$ is controlled by the Adaptive Clock (AClk). In addition, SL is set to V_{in} , BL is set to “0” and RLs are in high impedance.
- **Read or Sensing:** in this step, the sense amplifier reads the data stored in each VCMA-MTJ. SL is in high impedance and BL is set to “0”.

The switches and resistors presented in Figure 18 are responsible for the adaptive quantization resolution levels. With the resistors, different MTJs have different V_b . Thus, while some MTJs require

lower input voltages to turn on; others switch their state only with higher input voltages. The switches allow for the optimization of the QR by turning off the MTJs which are not used.

In Reference [9], the authors used 255 VCMA-MTJs to realize a range of quantization resolutions from 1-bit to 8-bit ADC operations. Their obtained results show that this AIQ leads to better power consumption compared to other CS ADC designs.

4.5. Sensors

With the increase of transistor scaling and power density, the temperature monitoring and the analysis of heating effects are very important, leading temperature sensors to become a relevant component in SoC. MTJ can also be used as a sensor resulting in high conversion, compact and low energy consumption devices. In Reference [73] an MTJ-based temperature sensor is proposed (see Figure 19). The SOT switching mechanisms are used to stochastically switch the MTJ state according to the operating temperature in the presence of thermal noise. The MTJ probabilistic switching characteristics of the MTJ can be given by the Landau-Lifshitz-Gilbert (LLG) equation [73]:

$$\frac{d\hat{m}}{dt} = -\gamma(\hat{m} \times \mathbf{H}_{eff}) + \alpha(\hat{m} \times \frac{d\hat{m}}{dt}) + \frac{1}{qN_s}(\hat{m} \times \mathbf{I}_s \times \hat{m}), \quad (14)$$

where \hat{m} is the vector of free layer magnetization, $\gamma = \frac{2\mu_B\mu_0}{\hbar}$ is the gyromagnetic ratio for electron, μ_B is Bohr magneton, \mathbf{H}_{eff} is the effective magnetic field including the shape anisotropy field for elliptic disks, α is Gilbert's damping ratio, $N_s = \frac{M_s V}{\mu_B}$ is the number of spins in a free layer of volume V , M_s is saturation magnetization and \mathbf{I}_s is the spin current generated by the heavy metal layer.

As can be seen in Figure 19, the sensor MTJ (MTJ2) and the reference MTJ (MTJ1—fixed at its AP state) form a voltage divider circuit. The switching probability ($P_{SW}(T)$) is given by the inverter output. The control signals RD and WR active the read and write current paths respectively. In the write operation, WR is on and then the I_{bias} current probabilistically switches the magnet depending on the temperature. On the other hand, during the read operations, RD is on and the sensor MTJ final state is determined. Between the write and the read operations, there is a “relaxation” period (T_{RELAX}) in order to stabilize the magnetization directions after the write operation. This MTJ-based temperature sensor achieves better results than state-of-the-art CMOS temperature sensors in terms of throughput and energy consumption [73].

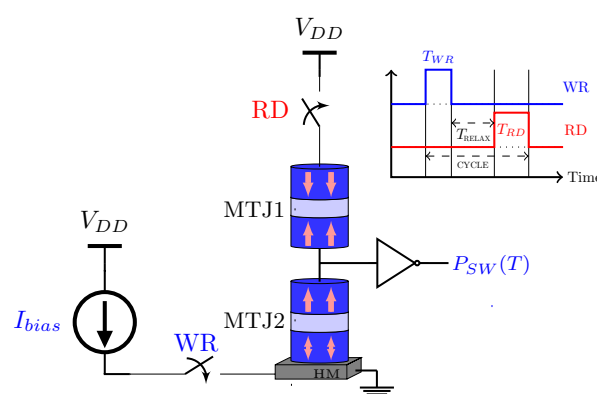


Figure 19. The MTJ-based temperature sensor proposed in Reference [73].

Regarding a frequency sensor, Reference [74] proposes an MTJ-based microwave detector that can be used, for example, as a spectrum analyzer. The ferromagnetic resonance in MTJs can determine the microwave frequency. With this, the mixer circuit is not required in conventional RF diode detection.

In order to monitor at the IC level, MTJ full Wheatstone bridges are proposed in Reference [75]. As can be seen in Figure 20, the currents in MTJ1 and MTJ3 flows in the opposite direction than it does in MTJ2 and MTJ4. Therefore, depending on the sign of the current through terminals A and B, the

resistance of MTJ1 and MTJ3 increases/decreases, while MTJ2 and MTJ4 change in the opposite way, leading to the Wheatstone bridge operation.

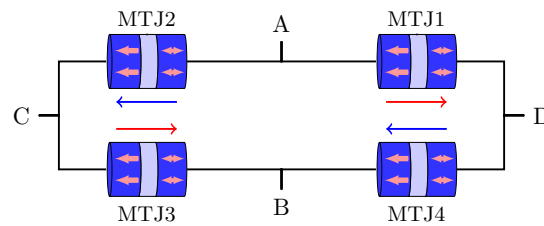


Figure 20. Full bridge configuration.

As we have shown, several papers have addressed MTJ applications. However, there are still many other domains where MTJ can be applied. Using, for example, its stochastic behavior, MTJ can also be used as a memristive probabilistic device and to implement the activation function [76] for Spiking Neural Networks (SNNs). As SNN intends to mimic the computational efficiency of the human brain, non-volatile resistive memories can be found in the literature to mimic a stochastic one-bit synapse [76,77]. The MTJ conductance is used to modulate the voltage spike produced by a pre-neuron resulting in a post-synaptic current.

5. Conclusions

The characteristics of MTJs make this type of device suitable in various areas. This paper provided a review of several works where MTJs were used to improve circuit consumption, area and efficiency. The text showed, in particular, that MTJ has been considered a promising alternative for the development of universal memory. Furthermore, the reported works show that MTJ can also play an important role in several other fundamental blocks such as comparators, ADC and sensors.

The use of MTJ is quite interesting in many applications where it can replace multiple transistors. These transistors, at nanometers scale, face problems of increasing static power consumption. Unfortunately, MTJ is a technology that still requires a great deal of development and only a few companies produce it. The simultaneous control of several MTJ parameters is one of the challenges of large-scale use of MTJ-based devices, for example, maintaining simultaneously high thermal stability and low switching current. Moreover, there are reliability challenges involving write and read failures. Indeed, process variations can significantly influence bit errors. On the other hand, scaling to smaller cell sizes is difficult, due to several factors such as the magnitude of the required switching currents. Despite these difficulties, the simulation results are promising regarding the advantages of using MTJ. In addition, new effects related to the switching of the magnetic state of MTJ devices have been studied and more optimal materials to be used in the MTJ structure have been developed.

Author Contributions: The manuscript was written by N.M. and E.M.; L.N. and H.C. supervised the work. All the authors reviewed the article. All authors have read and agree to the published version of the manuscript.

Funding: This research was funded by Télécom Paris and the Fondation de Coopération Scientifique Campus Paris Saclay (Project SpinTCAM, convention FCS 2017-0053D).

Conflicts of Interest: The authors declare no conflict of interest.

Abbreviations

The following abbreviations are used in this manuscript:

ADC	Analog to Digital Converter
AIC	Analog-to-Information Converter
AIQ	Adaptive Intermittent Quantizer
AP	Anti-parallel
AQR	Adaptive Quantization Rate

BL	Bit-line
CMOS	Complementary Metal Oxide Semiconductor
CPU	Central Processing Unit
CS	Compressive Sensing
DRAM	Dynamic Random-Access Memory
FA	Full Adder
FF	Flip-Flop
FL	Free Layer
FPGA	Field Programmable Gate Array
GMR	Giant Magnetoresistance
HM	Heavy Metal
IC	Integrated Circuits
IoT	Internet of Things
LFSR	Linear Feedback Shift Register
LUT	Look-up Table
MRAM	Magnetic Random Access Memory
MTJ	Magnetic tunnel junction
NUS	Non-Uniform Sampling
NVM	Non-Volatile Memory
P	Parallel
PL	Pinned Layer
PMA	Perpendicular Magnetic Anisotropy
QR	Quantization Resolution
RL	Read Line
SET	Single-Event Transient
SHM	Spin Hall Metal
SL	Source Line
SoC	System On Chip
SR	Sampling Rate
SRAM	Static Random-Access Memory
STT	Spin Transfer Torque
SOT	Spin-Orbit Torque
TMR	Tunnel Magnetoresistance
VCMA	Voltage-Controlled Magnetic Anisotropy
VCSO	Voltage-Controlled Stochastic Oscillator
WL	Word-line

References

1. Baibich, M.N.; Broto, J.M.; Fert, A.; Van Dau, F.N.; Petroff, F.; Etienne, P.; Creuzet, G.; Friederich, A.; Chazelas, J. Giant Magnetoresistance of (001)Fe/(001)Cr Magnetic Superlattices. *Phys. Rev. Lett.* **1988**, *61*, 2472–2475. [[CrossRef](#)]
2. Ennen, I.; Kappe, D.; Rempel, T.; Glenske, C.; Hütten, A. Giant Magnetoresistance: Basic Concepts, Microstructure, Magnetic Interactions and Applications. *Sensors* **2016**, *16*, 904. [[CrossRef](#)]
3. Gregg, J.F.; Petej, I.; Jouguelet, E.; Dennis, C. Spin electronics a review. *J. Phys. Appl. Phys.* **2002**, *35*, R121–R155. [[CrossRef](#)]
4. Peng, S.; Zhang, Y.; Wang, M.; Zhang, Y.; Zhao, W. *Magnetic Tunnel Junctions for Spintronics: Principles and Applications*; Wiley: Hoboken, NJ, USA, 2014; pp. 1–16. [[CrossRef](#)]
5. Chappert, C.; Fert, A.; Dau, F.N.V. The emergence of spin electronics in data storage. *Nat. Mater.* **2007**, *6*, 813–823. [[CrossRef](#)]
6. Qoutb, A.G.; Friedman, E.G. MTJ Magnetization Switching Mechanisms for IoT Applications. In Proceedings of the 2018 on Great Lakes Symposium on VLSI, Chicago, IL, USA, 23–25 May 2018; pp. 347–352. [[CrossRef](#)]
7. Cai, H.; Wang, Y.; Naviner, L.A.D.B.; Zhao, W. Robust Ultra-Low Power Non-Volatile Logic-in-Memory Circuits in FD-SOI Technology. *IEEE Trans. Circuits Syst. Regul. Pap.* **2017**, *64*, 847–857. [[CrossRef](#)]

8. Zarei, A.; Safaei, F. Power and area-efficient design of VCMA-MRAM based full-adder using approximate computing for IoT applications. *Microelectron. J.* **2018**, *82*, 62–70. [[CrossRef](#)]
9. Salehi, S.; Mashhadi, M.B.; Zaeemzadeh, A.; Rahnavard, N.; DeMara, R.F. Energy-Aware Adaptive Rate and Resolution Sampling of Spectrally Sparse Signals Leveraging VCMA-MTJ Devices. *IEEE J. Emerg. Sel. Top. Circuits Syst.* **2018**, *8*, 679–692. [[CrossRef](#)]
10. Chakraborty, I.; Agrawal, A.; Roy, K. Design of a Low-Voltage Analog-to-Digital Converter Using Voltage-Controlled Stochastic Switching of Low Barrier Nanomagnets. *IEEE Magn. Lett.* **2018**, *9*, 1–5. [[CrossRef](#)]
11. Marques, E.C.; Maciel, N.; Naviner, L.; Cai, H.; Yang, J. A Review of Sparse Recovery Algorithms. *IEEE Access* **2019**, *7*, 1300–1322. [[CrossRef](#)]
12. Zhang, D.; Zeng, L.; Zhang, Y.; Klein, J.O.; Zhao, W. Reliability-Enhanced Hybrid CMOS/MTJ Logic Circuit Architecture. *IEEE Trans. Magn.* **2017**, *53*, 1–5. [[CrossRef](#)]
13. Deng, E.; Kang, W.; Zhang, Y.; Klein, J.; Chappert, C.; Zhao, W. Design Optimization and Analysis of Multicontext STT-MTJ/CMOS Logic Circuits. *IEEE Trans. Nanotechnol.* **2015**, *14*, 169–177. [[CrossRef](#)]
14. Kang, W.; Deng, E.; Klein, J.; Zhang, Y.; Zhang, Y.; Chappert, C.; Ravelosona, D.; Zhao, W. Separated Precharge Sensing Amplifier for Deep Submicrometer MTJ/CMOS Hybrid Logic Circuits. *IEEE Trans. Magn.* **2014**, *50*, 1–5. [[CrossRef](#)]
15. Cai, H.; Wang, Y.; de Barros Naviner, L.A.; Yang, J.; Zhao, W. Exploring Hybrid STT-MTJ/CMOS Energy Solution in Near-/Sub-Threshold Regime for IoT Applications. *IEEE Trans. Magn.* **2018**, *54*, 1–9. [[CrossRef](#)]
16. Berger, L. Emission of spin waves by a magnetic multilayer traversed by a current. *Phys. Rev. B* **1996**, *54*, 9353–9358. [[CrossRef](#)]
17. Senni, S.; Torres, L.; Sassatelli, G.; Gamatie, A.; Mussard, B. Exploring MRAM Technologies for Energy Efficient Systems-On-Chip. *IEEE J. Emerg. Sel. Top. Circuits Syst.* **2016**, *6*, 279–292. [[CrossRef](#)]
18. Wang, Y.; Zhang, Y.; Deng, E.; Klein, J.O.; Naviner, L.A.B.; Zhao, W. Compact model of magnetic tunnel junction with stochastic spin transfer torque switching for reliability analyses. *Microelectron. Reliab.* **2014**, *54*, 1774–1778. [[CrossRef](#)]
19. Cai, H.; Wang, Y.; de Barros Naviner, L.A.; Zhao, W. Low Power Magnetic Flip-Flop Optimization With FDSOI Technology Boost. *IEEE Trans. Magn.* **2016**, *52*, 1–7. [[CrossRef](#)]
20. Kang, W.; Ran, Y.; Zhang, Y.; Lv, W.; Zhao, W. Modeling and Exploration of the Voltage-Controlled Magnetic Anisotropy Effect for the Next-Generation Low-Power and High-Speed MRAM Applications. *IEEE Trans. Nanotechnol.* **2017**, *16*, 387–395. [[CrossRef](#)]
21. Maruyama, T.; Shiota, Y.; Nozaki, T.; Ohta, K.; Toda, N.; Mizuguchi, M.; Tulapurkar, A.A.; Shinjo, T.; Shiraishi, M.; Mizukami, S.; et al. Large voltage-induced magnetic anisotropy change in a few atomic layers of iron. *Nat. Nanotechnol.* **2009**, *4*, 158–161. [[CrossRef](#)]
22. Wang, W.; Li, M.; Hageman, S.; Chien, C. Electric-field-assisted switching in magnetic tunnel junctions. *Nat. Mater.* **2012**, *11*, 64–68. [[CrossRef](#)]
23. Barnes, S.E.; Ieda, J.I.; Maekawa, S. Rashba spin-orbit anisotropy and the electric field control of magnetism. *Sci. Rep.* **2014**, *4*, 1–5. [[CrossRef](#)] [[PubMed](#)]
24. Velev, J.P.; Jaswal, S.S.; Tsymbal, E.Y. Multi-ferroic and magnetoelectric materials and interfaces. *Philos. Trans. Math. Phys. Eng. Sci.* **2011**, *369*, 3069–3097. [[CrossRef](#)] [[PubMed](#)]
25. Cai, H.; Wang, Y.; Kang, W.; Naviner, L.; Shan, W.; Yang, J.; Zhao, W. Enabling Resilient Voltage-Controlled MeRAM Using Write Assist Techniques. In Proceedings of the 2018 IEEE International Symposium on Circuits and Systems (ISCAS), Florence, Italy, 27–30 May 2018; pp. 1–5. [[CrossRef](#)]
26. Kang, W.; Chang, L.; Zhang, Y.; Zhao, W. Voltage-controlled MRAM for working memory: Perspectives and challenges. In Proceedings of the Design, Automation Test in Europe Conference Exhibition (DATE), Lausanne, Switzerland, 27–31 March 2017; pp. 542–547. [[CrossRef](#)]
27. Apalkov, D.; Dieny, B.; Slaughter, J.M. Magnetoresistive Random Access Memory. *Proc. IEEE* **2016**, *104*, 1796–1830. [[CrossRef](#)]
28. Wang, Z.; Li, Z.; Wang, M.; Wu, B.; Zhu, D.; Zhao, W. Field-free spin-orbit-torque switching of perpendicular magnetization aided by uniaxial shape anisotropy. *Nanotechnology* **2019**, *30*, 375202. [[CrossRef](#)]
29. Dieny, B.; Sousa, R.; Herault, J.; Pappas, C.; Prenat, G.; Ebels, U.; Houssameddine, D.; Rodmacq, B.; Auffret, S.; Buda-Prejbeanu, L.; et al. Spin-Transfer Effect and its Use in Spintronic Components. *Int. J. Nanotechnol.* **2010**, *7*. [[CrossRef](#)]

30. Åkerman, J. Toward a Universal Memory. *Science* **2005**, *308*, 508–510. [[CrossRef](#)]
31. Hosomi, M.; Yamagishi, H.; Yamamoto, T.; Bessho, K.; Higo, Y.; Yamane, K.; Yamada, H.; Shoji, M.; Hachino, H.; Fukumoto, C.; et al. A novel nonvolatile memory with spin torque transfer magnetization switching: Spin-RAM. In Proceedings of the IEEE International Electron Devices Meeting, 2005, IEDM Technical Digest, Washington, DC, USA, 5–7 December 2005; pp. 459–462. [[CrossRef](#)]
32. Wang, Z.; Zhang, L.; Wang, M.; Wang, Z.; Zhu, D.; Zhang, Y.; Zhao, W. High-Density NAND-Like Spin Transfer Torque Memory With Spin Orbit Torque Erase Operation. *IEEE Electron Device Lett.* **2018**, *39*, 343–346. [[CrossRef](#)]
33. Lin, C.J.; Kang, S.H.; Wang, Y.J.; Lee, K.; Zhu, X.; Chen, W.C.; Li, X.; Hsu, W.N.; Kao, Y.C.; Liu, M.T.; et al. 45nm low power CMOS logic compatible embedded STT MRAM utilizing a reverse-connection 1T/1MTJ cell. In Proceedings of the 2009 IEEE International Electron Devices Meeting (IEDM), Baltimore, MD, USA, 7–9 December 2009; pp. 1–4. [[CrossRef](#)]
34. Cubukcu, M.; Boulle, O.; Drouard, M.; Garello, K.; Onur Avci, C.; Mihai Miron, I.; Langer, J.; Ocker, B.; Gambardella, P.; Gaudin, G. Spin-orbit torque magnetization switching of a three-terminal perpendicular magnetic tunnel junction. *Appl. Phys. Lett.* **2014**. [[CrossRef](#)]
35. Fong, X.; Kim, Y.; Venkatesan, R.; Choday, S.H.; Raghunathan, A.; Roy, K. Spin-Transfer Torque Memories: Devices, Circuits, and Systems. *Proc. IEEE* **2016**, *104*, 1449–1488. [[CrossRef](#)]
36. Shiota, Y.; Nozaki, T.; Bonell, F.; Murakami, S.; Shinjo, T.; Suzuki, Y. Induction of coherent magnetization switching in a few atomic layers of FeCo using voltage pulses. *Nat. Mater.* **2012**, *11*, 39–43. [[CrossRef](#)]
37. Sharmin, S.; Jaiswal, A.; Roy, K. Modeling and design space exploration for bit-cells based on voltage-assisted switching of magnetic tunnel junctions. *IEEE Trans. Electron Devices* **2016**, *63*, 3493–3500. [[CrossRef](#)]
38. Wang, S.; Lee, H.; Ebrahimi, F.; Amiri, P.K.; Wang, K.L.; Gupta, P. Comparative Evaluation of Spin-Transfer-Torque and Magnetoelectric Random Access Memory. *IEEE J. Emerg. Sel. Top. Circuits Syst.* **2016**, *6*, 134–145. [[CrossRef](#)]
39. Zhang, H.; Kang, W.; Wang, Z.; Deng, E.; Zhang, Y.; Zhao, W. High-Density and Fast-Configuration Non-Volatile Look-Up Table Based on NAND-Like Spintronic Memory. In Proceedings of the 2018 IEEE Asia Pacific Conference on Circuits and Systems (APCCAS), Chengdu, China, 26–30 October 2018; pp. 382–385. [[CrossRef](#)]
40. Tsou, Y.; Chiu, J.; Shih, H.; Liu, C.W. Write Margin Analysis of Spin-Orbit Torque Switching Using Field-Assisted Method. *IEEE J. Explor.-Solid-State Comput. Devices Circuits* **2019**, *1*. [[CrossRef](#)]
41. Garello, K.; Yasin, F.; Hody, H.; Couet, S.; Souriau, L.; Sharifi, S.H.; Swerts, J.; Carpenter, R.; Rao, S.; Kim, W.; et al. Manufacturable 300mm platform solution for Field-Free Switching SOT-MRAM. In Proceedings of the 2019 Symposium on VLSI Technology, Kyoto, Japan, 9–14 June, 2019; pp. T194–T195. [[CrossRef](#)]
42. Jan, G.; Thomas, L.; Le, S.; Lee, Y.; Liu, H.; Zhu, J.; Iwata-Harms, J.; Patel, S.; Tong, R.; Sundar, V.; et al. Demonstration of Ultra-Low Voltage and Ultra Low Power STT-MRAM designed for compatibility with 0x node embedded LLC applications. In Proceedings of the 2018 IEEE Symposium on VLSI Technology, Honolulu, HI, USA, 18–22 June 2018; pp. 65–66. [[CrossRef](#)]
43. Garello, K.; Yasin, F.; Kar, G.S. Spin-Orbit Torque MRAM for ultrafast embedded memories: From fundamentals to large scale technology integration. In Proceedings of the 2019 IEEE 11th International Memory Workshop (IMW), Monterey, CA, USA, 12–15 May 2019; pp. 1–4. [[CrossRef](#)]
44. Li, X.; Lee, A.; Razavi, S.; Wu, H.; Wang, K. Voltage-controlled magnetoelectric memory and logic devices. *MRS Bull.* **2018**, *43*, 970–977. [[CrossRef](#)]
45. Kobayashi, D.; Hirose, K.; Makino, T.; Onoda, S.; Ohshima, T.; Ikeda, S.; Sato, H.; Enobio, E.C.I.; Endoh, T.; Ohno, H. Soft errors in 10-nm-scale magnetic tunnel junctions exposed to high-energy heavy-ion radiation. *Jpn. J. Appl. Phys.* **2017**, *56*, 0802B4. [[CrossRef](#)]
46. Yang, J.; Wang, P.; Zhang, Y.; Cheng, Y.; Zhao, W.; Chen, Y.; Li, H.H. Radiation-Induced Soft Error Analysis of STT-MRAM: A Device to Circuit Approach. *IEEE Trans. Comput.-Aided Des. Integr. Circuits Syst.* **2016**, *35*, 380–393. [[CrossRef](#)]
47. Maciel, N.; Marques, E.C.; Naviner, L.; Cai, H.; Yang, J. Voltage-Controlled Magnetic Anisotropy MeRAM Bit-Cell over Event Transient Effects. *J. Low Power Electron. Appl.* **2019**, *9*, 15. [[CrossRef](#)]
48. Wang, B.; Wang, Z.; Hu, C.; Zhao, Y.; Zhang, Y.; Zhao, W. Radiation-Hardening Techniques for Spin Orbit Torque-MRAM Peripheral Circuitry. *IEEE Trans. Magn.* **2018**, *54*, 1–5. [[CrossRef](#)]

49. Maciel, N.; Marques, E.; Naviner, L.; Cai, H.; Yang, J. Reliability Analysis of NAND-Like Spintronic Memory. *Microelectron. Reliab.* **2019**. [[CrossRef](#)]
50. Deng, E. Design and Development of Low-Power and Reliable Logic Circuits Based on Spin-Transfer Torque Magnetic Tunnel Junctions. Ph.D. Thesis, Université Grenoble Alpes, Grenoble, France, 10 February 2017.
51. Kuon, I.; Tessier, R.; Rose, J. *FPGA Architecture: Survey and Challenges*; Foundations and Trends in Electronic Design Automation Series; Foundations and Trends®: Delft, The Netherlands, 2008.
52. Salehi, S.; Zand, R.; DeMara, R.F. Clockless Spin-based Look-Up Tables with Wide Read Margin. In Proceedings of the 2019 on Great Lakes Symposium on VLSI, Tysons Corner, VA, USA, 9–11 May 2019; pp. 363–366. [[CrossRef](#)]
53. Zand, R.; Roohi, A.; Salehi, S.; DeMara, R.F. Scalable Adaptive Spintronic Reconfigurable Logic Using Area-Matched MTJ Design. *IEEE Trans. Circuits Syst. II Express Briefs* **2016**, *63*, 678–682. [[CrossRef](#)]
54. Zhao, W.; Belhaire, E.; Chappert, C.; Dieny, B.; Prenat, G. TAS-MRAM-Based Low-Power High-Speed Runtime Reconfiguration (RTR) FPGA. *ACM Trans. Reconfigurable Technol. Syst.* **2009**, *2*, 8:1–8:19. [[CrossRef](#)]
55. Huang, K.; Ha, Y.; Zhao, R.; Kumar, A.; Lian, Y. A Low Active Leakage and High Reliability Phase Change Memory (PCM) Based Non-Volatile FPGA Storage Element. *IEEE Trans. Circuits Syst. Regul. Pap.* **2014**, *61*, 2605–2613. [[CrossRef](#)]
56. Zand, R.; DeMara, R.F. Radiation-hardened MRAM-based LUT for non-volatile FPGA soft error mitigation with multi-node upset tolerance. *J. Phys. Appl. Phys.* **2017**, *50*, 505002. [[CrossRef](#)]
57. Attaran, A.; Sheaves, T.D.; Mugula, P.K.; Mahmoodi, H. Static Design of Spin Transfer Torques Magnetic Look Up Tables for ASIC Designs. In Proceedings of the 2018 on Great Lakes Symposium on VLSI, Chicago, IL, USA, 23–25 May 2018; pp. 507–510. [[CrossRef](#)]
58. Zhao, W.; Belhaire, E.; Javerliac, V.; Chappert, C.; Dieny, B. Evaluation of a Non-Volatile FPGA based on MRAM technology. In Proceedings of the 2006 IEEE International Conference on IC Design and Technology, Padova, Italy, 1–4 May 2006; pp. 1–4. [[CrossRef](#)]
59. Zhao, W.; Belhaire, E.; Chappert, C. Spin-MTJ based Non-volatile Flip-Flop. In Proceedings of the 2007 7th IEEE Conference on Nanotechnology (IEEE NANO), Hong Kong, China, 2–5 August 2007; pp. 399–402. [[CrossRef](#)]
60. Montesi, L.; Zilic, Z.; Hanyu, T.; Suzuki, D. Building Blocks to Use in Innovative Non-volatile FPGA Architecture Based on MTJs. In Proceedings of the 2012 IEEE Computer Society Annual Symposium on VLSI, Amherst, MA, USA, 19–21 August 2012; pp. 302–307. [[CrossRef](#)]
61. Onizawa, N.; Hanyu, T. Redundant STT-MTJ-based nonvolatile flip-flops for low write-error-rate operations. In Proceedings of the 2016 14th IEEE International New Circuits and Systems Conference (NEWCAS), Vancouver, BC, Canada, 26–29 June 2016; pp. 1–4. [[CrossRef](#)]
62. Iyengar, A.S.; Ghosh, S.; Jang, J. MTJ-Based State Retentive Flip-Flop With Enhanced-Scan Capability to Sustain Sudden Power Failure. *IEEE Trans. Circuits Syst. Regul. Pap.* **2015**, *62*, 2062–2068. [[CrossRef](#)]
63. Meng, H.; Wang, J.G.; Wang, J.P. A spintronics full adder for magnetic CPU. *IEEE Electron Device Lett.* **2005**, *26*, 360–362. [[CrossRef](#)]
64. Matsunaga, S.; Hayakawa, J.; Ikeda, S.; Miura, K.; Hasegawa, H.; Endoh, T.; Ohno, H.; Hanyu, T. Fabrication of a Nonvolatile Full Adder Based on Logic-in-Memory Architecture Using Magnetic Tunnel Junctions. *Appl. Phys. Express* **2008**, *1*. [[CrossRef](#)]
65. Gang, Y.; Zhao, W.; Klein, J.; Chappert, C.; Mazoyer, P. A High-Reliability, Low-Power Magnetic Full Adder. *IEEE Trans. Magn.* **2011**, *47*, 4611–4616. [[CrossRef](#)]
66. Jonsson, B.E. A survey of A/D-Converter performance evolution. In Proceedings of the 2010 17th IEEE International Conference on Electronics, Circuits and Systems, Athens, Greece, 12–15 December 2010; pp. 766–769. [[CrossRef](#)]
67. Jiang, Y.; Lv, Y.; Jamali, M.; Wang, J. Spin Analog-to-Digital Converter Using Magnetic Tunnel Junction and Spin Hall Effect. *IEEE Electron Device Lett.* **2015**, *36*, 511–513. [[CrossRef](#)]
68. Salehi, S.; DeMara, R.F. SLIM-ADC: Spin-based Logic-In-Memory Analog to Digital Converter leveraging SHE-enabled Domain Wall Motion devices. *Microelectron. J.* **2018**, *81*, 137–143. [[CrossRef](#)]
69. Murmann, B. ADC Performance Survey (1997–2019). Available online: <http://web.stanford.edu/~murmman/adcsurvey.html> (accessed on 15 October 2019).
70. El-Chammas, M.; Murmann, B. A 12-GS/s 81-mW 5-bit Time-Interleaved Flash ADC With Background Timing Skew Calibration. *IEEE J. Solid-State Circuits* **2011**, *46*, 838–847. [[CrossRef](#)]

71. Lee, H.; Grezes, C.; Lee, A.; Ebrahimi, F.; Khalili Amiri, P.; Wang, K.L. A Spintronic Voltage-Controlled Stochastic Oscillator for Event-Driven Random Sampling. *IEEE Electron Device Lett.* **2017**, *38*, 281–284. [[CrossRef](#)]
72. Salehi, S.; Zand, R.; Zaeemzadeh, A.; Rahnavard, N.; DeMara, R.F. AQuRate: MRAM-based Stochastic Oscillator for Adaptive Quantization Rate Sampling of Sparse Signals. In Proceedings of the 2019 on Great Lakes Symposium on VLSI, Tysons Corner, VA, USA, 9–11 May 2019; pp. 359–362. [[CrossRef](#)]
73. Sengupta, A.; Liyanagedera, C.M.; Jung, B.; Roy, K. Magnetic Tunnel Junction as an On-Chip Temperature Sensor. *Sci. Rep.* **2017**, *7*, 11764. [[CrossRef](#)]
74. Fan, X.; Chen, Y.; Bi, C.; Xie, Y.; Kolodzey, J.; Wilson, J.D.; Simons, R.N.; Zhang, H.; Xiao, J.Q. Magnetic tunnel junction-based on-chip microwave phase and spectrum analyzer. In Proceedings of the 2014 IEEE MTT-S International Microwave Symposium (IMS2014), Tampa, FL, USA, 1–6 June 2014; pp. 1–4. [[CrossRef](#)]
75. Cubells, M.D.; Reig, C.; De Marcellis, A.; Roldán, A.; Roldán, J.; Cardoso, S.; Freitas, P.P. Magnetic Tunnel Junction (MTJ) sensors for integrated circuits (IC) electric current measurement. *Sensors* **2013**. [[CrossRef](#)]
76. Vincent, A.F.; Larroque, J.; Locatelli, N.; Ben Romdhane, N.; Bichler, O.; Gamrat, C.; Zhao, W.S.; Klein, J.; Galdin-Retailleau, S.; Querlioz, D. Spin-Transfer Torque Magnetic Memory as a Stochastic Memristive Synapse for Neuromorphic Systems. *IEEE Trans. Biomed. Circuits Syst.* **2015**, *9*, 166–174. [[CrossRef](#)] [[PubMed](#)]
77. Srinivasan, G.; Sengupta, A.; Roy, K. Magnetic Tunnel Junction Based Long-Term Short-Term Stochastic Synapse for a Spiking Neural Network with On-Chip STDP Learning. *Sci. Rep.* **2016**, *6*, 29545. [[CrossRef](#)]



© 2019 by the authors. Licensee MDPI, Basel, Switzerland. This article is an open access article distributed under the terms and conditions of the Creative Commons Attribution (CC BY) license (<http://creativecommons.org/licenses/by/4.0/>).